IEEE Access
Multidisciplinary | Rapid Review | Open Access Journal

Received July 9, 2019, accepted July 22, 2019, date of publication July 25, 2019, date of current version September 30, 2019.

Digital Object Identifier 10.1109/ACCESS.2019.2931155

Assessing Rockburst Hazards Using a Self-Developed Real-Time Microseismic Monitoring System in a Deep-Sea Goldmine

DONG LI[1], JUNFEI ZHANG[2], CUNWEN WANG[3], YANG CHEN[4], AND DECHENG GE[4]

[1]School of Safety Engineering, North China Institute of Science and Technology, Beijing 101601, China
[2]School of Civil, Environmental and Mining Engineering, The University of Western Australia, Perth, WA 6009, Australia
[3]Shandong Energy Group Company Ltd., Jinan 250014, China
[4]School of Civil and Resources Engineering, University of Science and Technology Beijing, Beijing 100083, China

Corresponding author: Junfei Zhang (junfei.zhang@research.uwa.edu.au)

This work was supported in part by the State Key Research Development Program of China under Grant 2016YFC0801408, in part by the National Natural Science Foundation of China under Grant 51674014, and in part by the Key Project of National Natural Science Foundation under Grant 51634001.

ABSTRACT Deep-sea mining extracts ores on the ocean floor. During this process the sea water may flood into the mine due to rockburst hazards. This study proposes an effective method to assess rockburst hazards using a self-developed real-time microseismic monitoring system in Sanshandao goldmine (the first undersea mine in China). In addition, the wave dissimilation patterns of this mine have been elucidated by analyzing the signals obtained by the geophones embedded in a similar material model. The monitoring work started in December 2014 and ended in March 2015 in Sanshandao goldmine. To assess rockburst hazards, this study proposes several indexes including spatial-temporal distribution of microseismic events, microseismic activity rate, energy release rate, continuity index, and average daily energy. The results show that the surrounding rock went through the stationary, active, secondary stationary, and secondary active periods before rockburst occurrence. Compared with the stationary period, a sudden change of the continuity index and average daily energy can be observed in the active period in which minor rockbursts constantly occurred. Rockburst accidents are very likely to occur in the secondary active period. However, before this period, there usually exists a secondary stationary period without rockburst risk. This study proposes a workflow for designing and applying microseismic monitoring systems.

INDEX TERMS Rock burst, similar material simulation, microseismic monitoring, elastic wave, propagation, wave dissimilation.

I. INTRODUCTION

Rockburst is a violent dynamic disaster caused by the sudden failure of the rock mass and is always associated with a large amount of seismic energy release [1]. Usually, rockburst hazards occur locally without influencing the general stability of the mine but can induce a variety of secondary hazards such as water burst, gas burst and dust explosion [2]–[4]. The past few decades have seen a number of rockburst accidents, which have caused many casualties and considerable economic loss [5], [6].

As some ore deposits are buried under the ocean floor, deep-sea mining has been developed to retrieve these minerals. In these mines, rockburst induced by mining activity may cause seawater to flood into the mine. Therefore, it is necessary to predict rockburst hazards in undersea mines in real time. By now, real-time microseismic monitoring techniques have been widely used during mining in many fields such as rock slope engineering [7], mining engineering [8], [9], tunneling [10] and hydrofracturing [11]–[13]. This technique can obtain spatial location, time, and magnitude of the microseismic events by analyzing the recorded acoustic signals. The mining-induced rock mass failure can then be predicted by using the obtained information [14]–[16]. Compared with the onshore deep mine, the water inflow of the deep-sea mine is much larger. The sea water is rich in halide, and therefore the vapor will corrode the devices in elevated temperatures. To address this problem,

The associate editor coordinating the review of this manuscript and approving it for publication was Bora Onat.

the devices of the microseismic monitoring system need to be specially designed for anti-corrosion purpose.

In the practice of microseismic monitoring, the static wave velocity is usually adopted; that is, the wave velocity between the focus and each geophone is equal, which results in a large location error [17]. The complex geological conditions in a mine will cause wave dissimilation such as attenuation of velocity and amplitude and disorder of first arrivals. There are three main factors that cause microseismic wave dissimilation: first, engineering defects, such as goafs, roadways, caverns, etc.; second, geological defects, such as faults, joints, bedding, subsided columns, etc., and third, lithological dissimilation, such as rock mass erosion, rock intrusion and lithological variation [18]. If the microseismic wave dissimilation is not taken into account, the fracture source of the rock cannot be located accurately [19], [20].

However, the rock mass in a mine is not ideal to study wave dissimilation quantitatively due to complex geological conditions. To address this problem, a similar material model is used to simulate the mine prototype in a laboratory scale. Generally, similar materials include sand, lime, gypsum and other additives. These materials are mixed at a certain proportion and then compressed and cured to simulate any rock formation in mines [21], [22]. The material mix proportions were studied by Hu *et al.*, which can be used as guidelines for designing similar material simulation experiments for coal mining [23].

In this study, a self-developed microseismic monitoring system is emloyed to monitor and predict rockburst disasters in Sanshandao goldmine during mining. In addition, to guide the future mining work in the unexplored zone of this mine with complex geological conditions, the wave dissimilation patterns have been elucidated using the similar material simulation test.

II. GEOLOGICAL SETTING OF SANSHANDAO GOLDMINE

Sanshandao goldmine is located in the northwestern edge of the Jiaodong Peninsula situated along the southeastern edge of the North China Craton (NCC) that is the oldest and largest craton in China [24], shown in **Fig. 1**. The northwestern part of the Jiaodong Peninsula is occupied by over 50% of mesozoic granitoids which hold more than 95% of gold resources. In this region, two principle deformation phases have been identified during the Mesozoic. One is distinguished by northwest–southeast oblique compression, probably associated with the subduction of the Izanagi–Pacific plate [25]. The other one contains half-graben basins, accompanied by intrusion of mafic dikes and hydrothermal gold mineralization.

The orebody strikes about N. (20–40°) E and dips approximately 35–70 degrees towards SE, and extends offshore into the Bohai Sea. The Sanshandao deposit is composed of four major lithological groups [26]: (1) Jurassic Linglong granite; (2) Archean Jiaodong Group; (3) Cretaceous Guojialing granodiorite and (4) Cretaceous mafic dikes (Fig. 1). The Sanshandao–Cangshang fault zone controls the Sanshandao

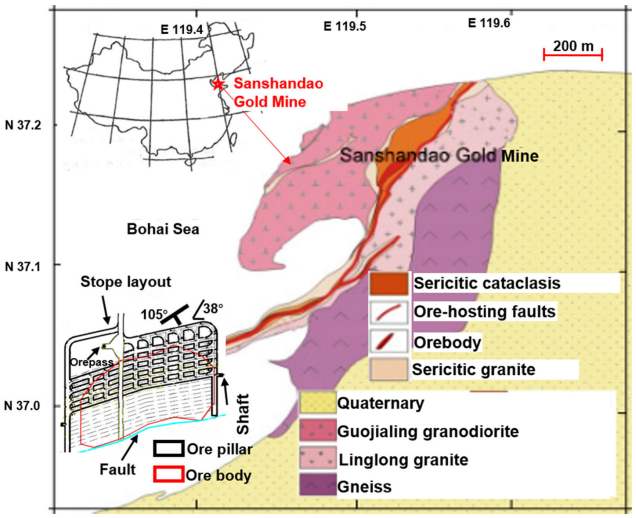

FIGURE 1. Geological profile and stope layout of Sanshandao goldmine.

FIGURE 2. Roadway damage caused by high shearing stress.

gold deposit with the Linglong granite/Guojialing granodiorite in the footwall and the Linglong granite in the hanging wall. Six orebodies with lenticular or tabular shape have been identified. The No. 1 orebody has the largest amount of reserves (69%) and is situated in the middle to upper part of the main fault footwall. This orebody is 1020 m long and 6.4 to 10.3 m thick with an approximate depth of 1450 m. The mining shaft has extended 1200 m from the surface and the operational depth will exceed 2000 m since a new large gold orebody with gold reserve larger than 500 t has been found by geological exploration [27].

In deep-sea mines, the rock strata may fracture due to high in-situ stress and mining activity, which may cause rockburst and mine flooding [28]. To address this problem, the goaf was backfilled using cemented paste backfill (CPB) with a much lower strength and density than the surrounding rock. The propagation patterns of microseismic waves in the particular geological conditions of undersea mines need to be further studied to develop and apply microseismic monitoring systems. The stope at level -780 m was mined using cut and fill method, as shown in **Fig. 1**.

According to the results of the geostress measurement, the maximum and minimum principal stresses are 33 MPa and 17 MPa, respectively. A large shearing stress is generated by the large difference of the two principal stresses, which may be the main cause of roadway deformation and failure [29], as shown in **Fig. 2**.

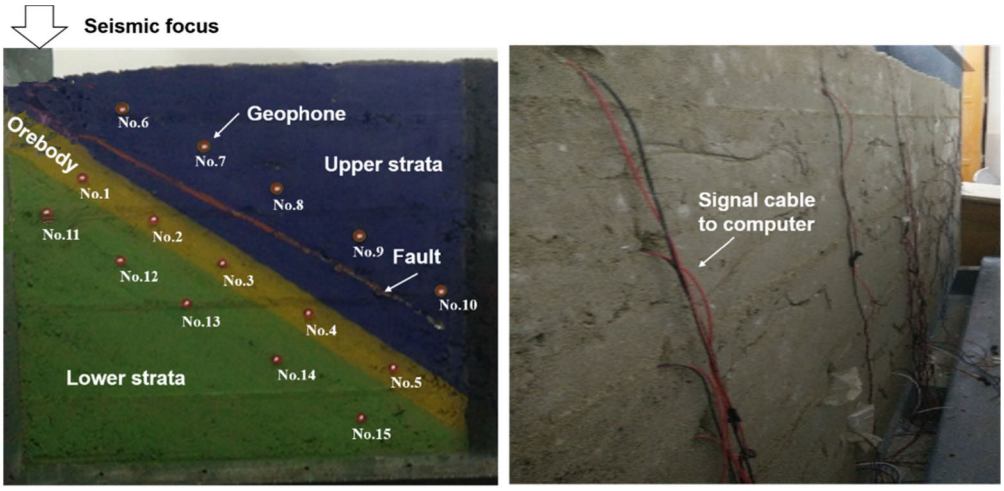

FIGURE 3. Experimental model: front (a) and back (b).

TABLE 1. Proportion of the similar materials.

Strata	Volume (m^3)	Sand (kg)	Lime (kg)	Gypsum (kg)	Dry weight (kg)	Water (kg)
Lower	0.18	300	52.5	22.5	374	41.60
Orebody	0.05	78	18.2	7.8	104	11.56
Upper 1	0.025	44	4	4	52	5.78
Upper 2	0.428	712	89	89	891	98.92
Total	0.683	1134	163.7	123.3	1421	157.85

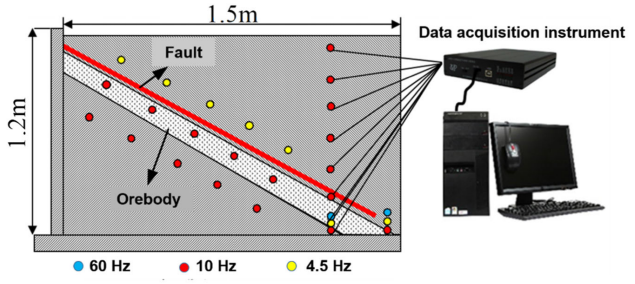

FIGURE 4. Schematic of the microseismic monitoring system.

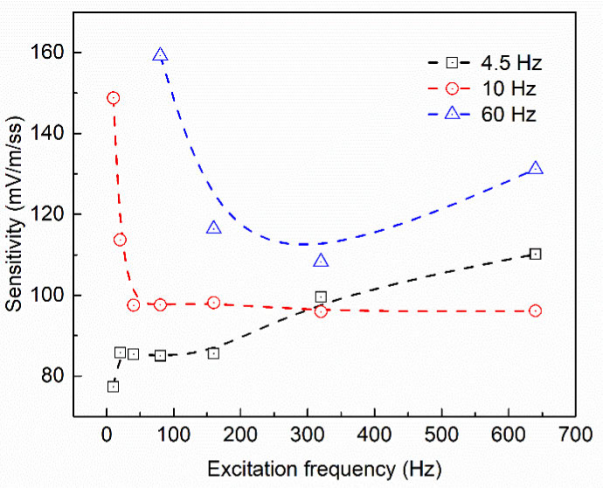

FIGURE 5. Sensitivity versus excitation frequency for three types of geophones.

III. SIMILAR MATERIAL SIMULATION TEST

A. SIMILARITY THEORY

A mine prototype can be downscaled to a much smaller experimental model based on similarity theory for convenient analysis. Geometric similarity, kinematic similarity and dynamic similarity must be satisfied when designing the similar material model [30]–[34]. To prepare the similar material model, dry sand was used as the aggregate; gypsum and lime were selected as the cementitious materials. Any rock formations with different strengths can be simulated by varying the proportions of the cementitious materials. The proportion of the materials (see **Table 1**) was calculated according to the previous literature [34]. Based on the prototype of Sanshandao goldmine, a similar model was designed in laboratory (**Fig. 3**). To fabricate the model, a mould was prefabricated using steel plates. Inside the model, one end of the steel plate was fixed, while the other end can be adjusted to adjust the

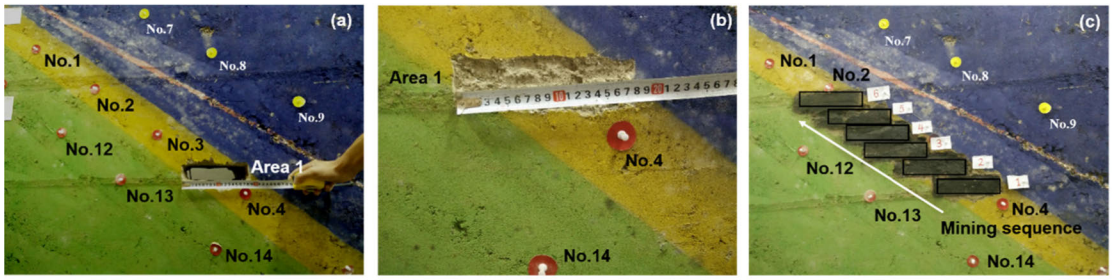

FIGURE 6. Excavation (a), backfill (b) and excavation sequence (c).

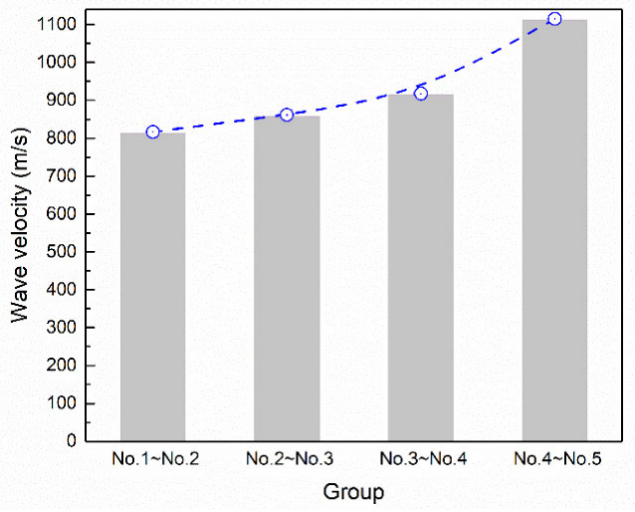

FIGURE 7. Wave velocity versus depth.

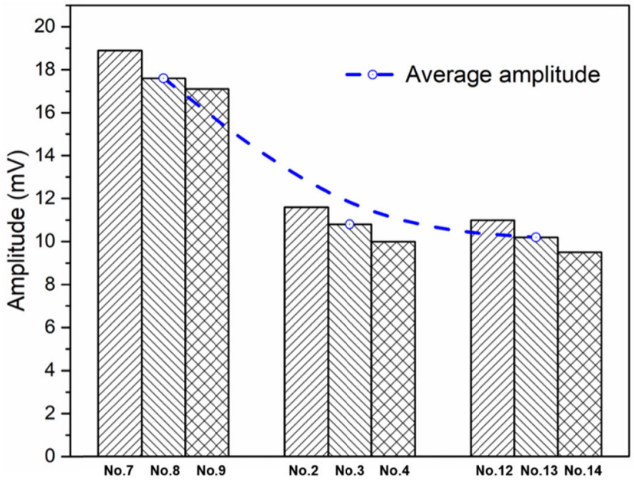

FIGURE 8. Variation of amplitudes influenced by the fault.

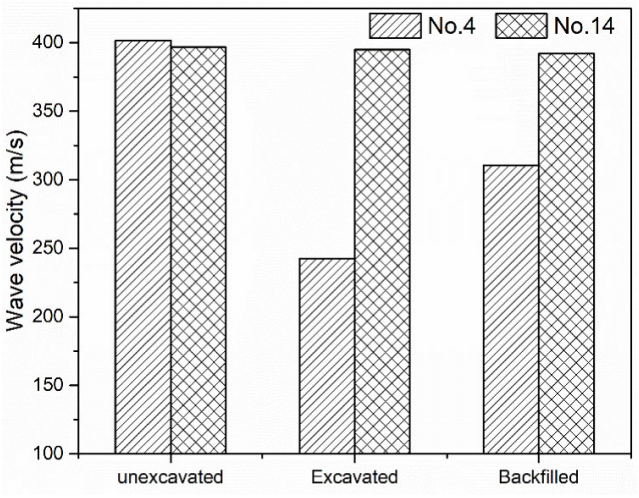

FIGURE 9. Wave velocity influenced by excavation.

dip of the strata. The required materials were weighed and then poured into a mixer for mixing (10 min) until a uniform paste was formed. The paste was then poured into the mould and compacted. After that, the model was placed in a moist room for curing with a relative humidity of 95 ± 5%, and an ambient temperature of 20 ± 1 °C for 28 days. In order to distinguish each rock stratum clearly, the front surface of the model were painted. In the meantime, circular pieces of paper were bonded to the positions where the geophones were buried (**Fig. 3**).

The large water content during curing may corrode the geophone and cause a short circuit between the positive and negative electrodes. To address this problem, the geophones were wax-sealed for waterproofing before use. Then the wax-sealed geophones were embedded in the model and connected to the data acquisition instrument by a signal cable. Acquired microseismic signals were analyzed in a desktop PC system (**Fig. 4**).

To achieve the best waveform during monitoring, three types of geophones with frequencies of 4.5 Hz (low sensitivity), 10 Hz (medium sensitivity) and 60 Hz (high sensitivity), were tested for their sensitivity (S) using the following formula by a vibration sensor calibrator:

$$S = \frac{(A_1 + A_2)}{2\sqrt{2}A} \tag{1}$$

where A_1 is the measured maximum amplitude; A_2 is the measured minimum amplitude; A is the excitation amplitude.

Fig. 5 shows the sensitivity of the geophone versus excitation frequency. It can be seen that the 10-Hz geophone has the best working linearity in the range between 30 Hz to 600 Hz. Therefore, the 10-Hz geophone (medium sensitivity) with a sampling rate of 8 k/s, sampling time of 2s, and number of compensation points of 1000 was used in this study.

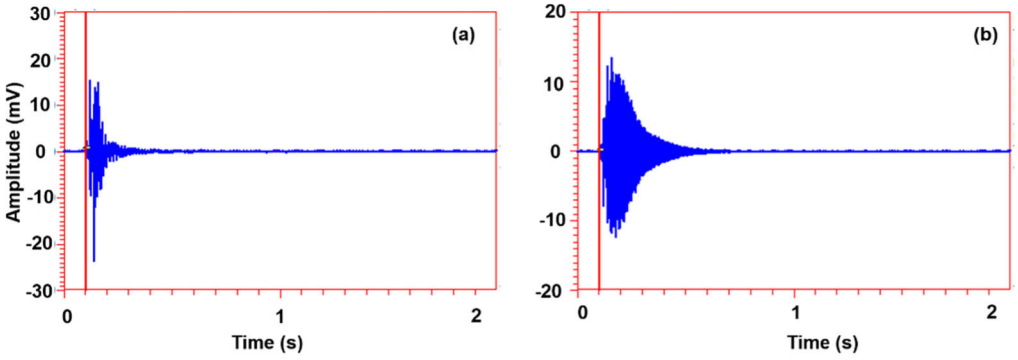

FIGURE 10. Waveform received by No.4 geophone after area 6 was mined (a), and area 1 was mined (b).

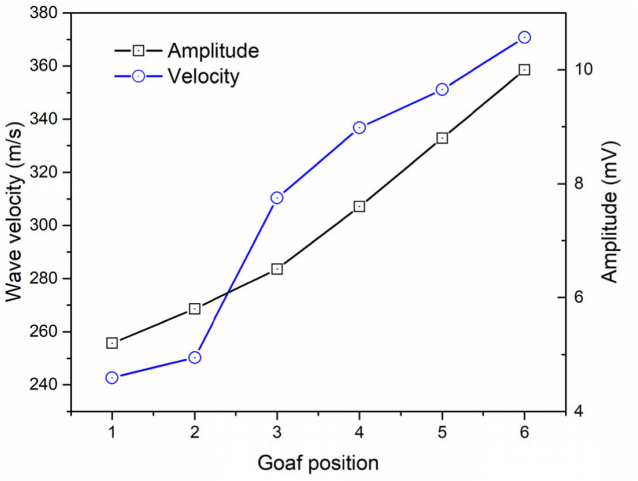

FIGURE 11. Variation of wave velocity and amplitude received by No. 4 geophone versus goaf position.

During monitoring, the seismic focus was knocked to generate elastic waves in the strata. The wave velocity (v) versus depth was firstly measured using the following equation:

$$v = \frac{s}{t} \tag{2}$$

where s is the propagation distance, and t is the propagation time. Then the influence of the fault was analyzed by comparing the amplitudes of the waves above the fault (No.7, No.8 and No.9) and below the fault (No.2, No.3, No.4, No.12, No.13 and No.14). Finally, the wave velocity influenced by excavation and backfill was studied. After area 1 was excavated (**Fig. 6**b), the wave velocities between the focus and No.4 geophone as well as the focus and No.14 geophone were compared, respectively to elucidate how the wave velocity is influenced by the goaf. Area 1 was then backfilled (**Fig. 6c**) and area 2 was excavated. Following this order, six areas were excavated and backfilled, successively. Before the next area was excavated, the previous one was backfilled. The wave velocity and amplitude versus excavation position was studied.

B. RESULTS OF THE SIMILAR MATERIAL SIMULATION TEST

To study the change of the wave velocity with depth in strata before excavation, the seismic focus was knocked to generate elastic waves. **Fig. 7** shows the change of the average wave velocity between two adjacent geophones during propagation. It can be seen that the average wave velocity increases with depth. The possible reason is that the density of the lower strata was larger due to better compaction.

Fig. 8 shows the variation of wave amplitudes received by the geophones under the influence of the fault. It can be seen that in each group the amplitude decreases with increasing the distance from the seismic source. In addition, it can be observed that after the elastic waves propagated through the fault to the geophones in the orebody (No.2, No.3 and No.4) and lower strata (No.12, No.13 and No.14), its amplitude decreases significantly. This is probably due to the energy attenuation caused by the loose medium in the fault [35], [36].

As can be seen from **Fig. 9**, before excavation, the wave velocity between No. 4 and the seismic focus is slightly larger than that between No.14 and the seismic focus. However, after mining, the former (closer to the goaf) velocity decreases significantly. This indicates that the goaf can cause large velocity attenuation to the wave during propagation. After backfill, the velocity increases again but is smaller than the original velocity as the density of the backfill material is smaller than that of the rock. The influence of the position of the goaf on the wave propagation is also studied. It should be noted that the former goaf had been backfilled before the next goaf was formed. It is found that the tail and duration of the waveform is elongated with increasing the distance between the goaf and the geophone (**Fig. 10**). In addition, both the amplitude and velocity increase with increasing the distance from the goaf (**Fig. 11**), indicating significance influence of the goaf to the nearby geophones.

The obtained propagation patterns are used to guide the deployment of the geophones in the mine. The influence of geological defects such as faults and goafs on elastic waves has been considered when installing geophones in the stope. In addition, the propagation patterns of microseismic waves

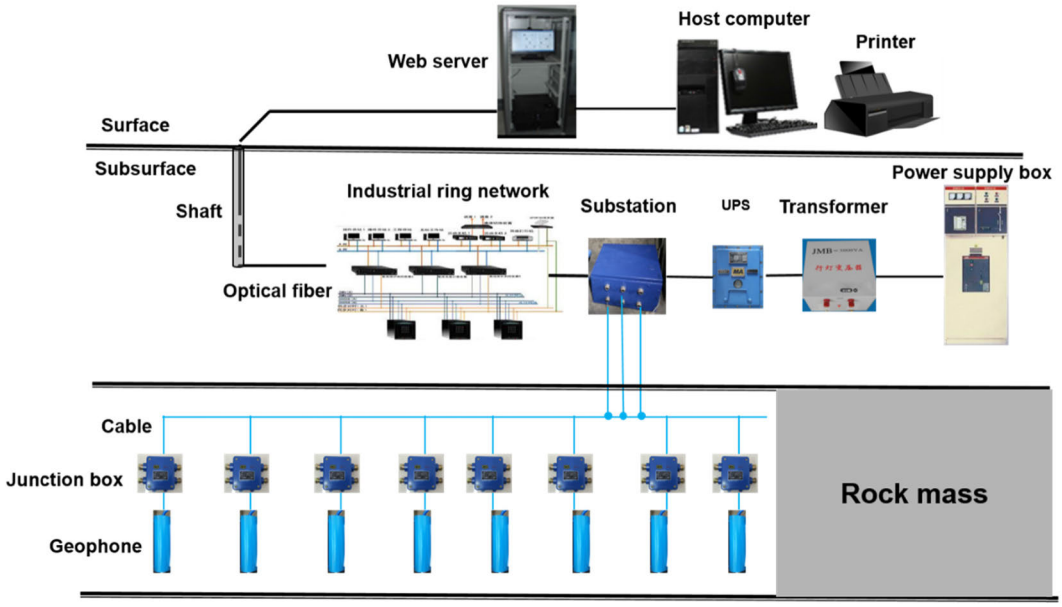

FIGURE 12. Configuration of the microseismic monitoring system at Sanshandao goldmine.

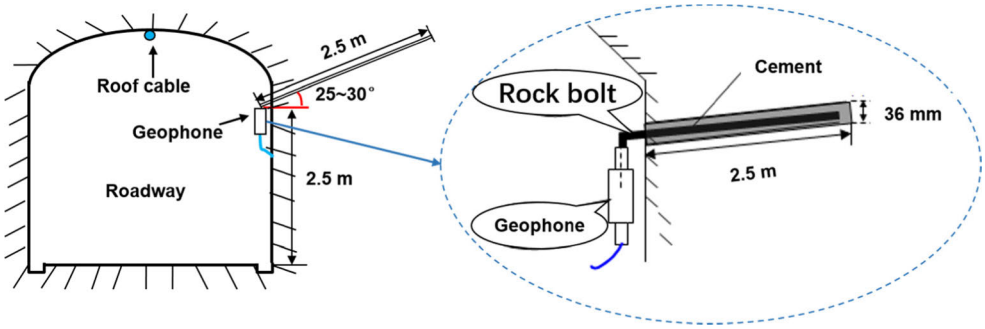

FIGURE 13. Installation of geophones.

can be used to detect undiscovered geological structure during future mining.

IV. MICROSEISMIC MONITORING IN SANSHANDAO GOLDMINE

A. DEVELOPMENT OF THE MICROSEISMIC MONITORING SYSTEM

1) HARDWARE STRUCTURE OF THE MICROSEISMIC MONITORING SYSTEM

The microseismic monitoring system was developed by our group and installed in Sanshandao goldmine (see **Fig. 12**). The system is composed of ten uniaxial geophones, a substation for data acquisition and processing, power supply and signal transmission cables. The maximum output, frequency and sensitivity of the geophones are −5V∼+5V, 5–50 kHz and 30 V/g, respectively. The substation containing a 24-bit analog-to-digital (A/D) converter has an acquisition of 20000 Hz. The geophones were installed at the end of the rock bolt at a height of 2.5 m from the floor. The rock bolts (2.5 m in length) were anchored in boreholes on the sidewalls using rapid-hardening hydraulic cement. The included angle between the borehole and the horizontal direction is 25∼30° (see **Fig. 13**). This system includes the underground part and above ground part. The underground part is composed of geophones, monitoring substation and monitoring host computers. Each substation has 12 monitoring channels which can connect 12 geophones. During monitoring, the elastic waves generated by rock fractures are detected by the geophones and transmitted through signal cables in the form of analog signals. Then the analog signals are digitized in the substation and transmitted into the web server through optical fibers and the industrial ring net. The digital data are then automatically recorded and displayed in the host computer.

2) SOFTWARE STRUCTURE OF THE MICROSEISMIC SYSTEM

The software system consists of the data acquisition software, data processing software and locating software. The data acquisition software is used to monitor and record the microseismic events. The data processing software is able to display microseismic waves, pickup first arrivals, and calculate microseismic energy. The function of the locating

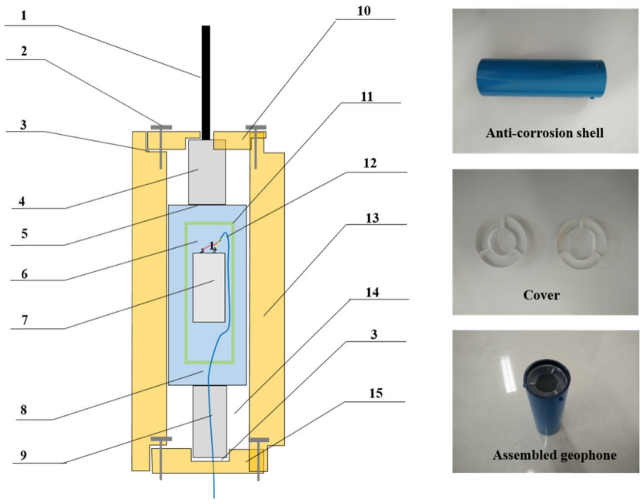

FIGURE 14. The shell of the anti-corrosion geophone: 1— anchor bolt; 2— screw; 3— rubber gasket; 4— upper joint pin; 5— inner metal shell; 6— Acrylic AB Adhesive; 7— Geophone chip; 8— acrylic AB adhesive; 9— lower joint pin; 10— upper cover; 11— plastic isolating frame; 12— cable; 13— outer anti-corrosion shell; 14— Vaseline; 15— lower cover.

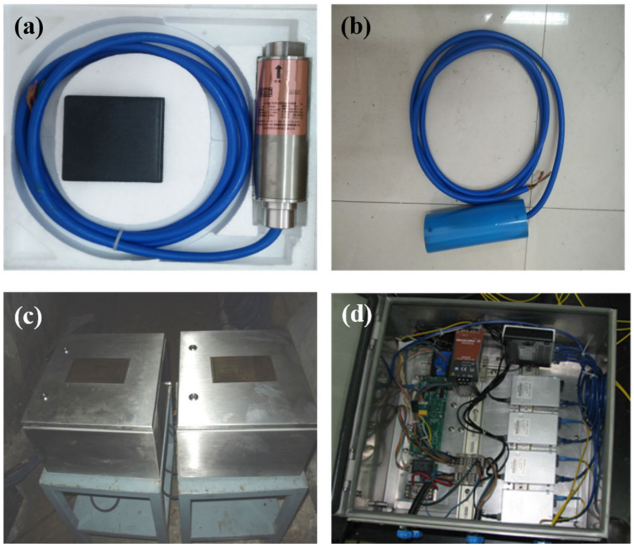

FIGURE 15. Bare Geophone (a); geophone with anticorrosion shell (b); packaged underground monitoring station (c) and inner structure of the monitoring station (d).

software is to display the microseismic events based on its occurring time, space and energy.

B. ANTICORROSIVE DESIGN OF MONITORING EQUIPMENT

As stated before, the inflow of the sea water rich in halide will corrode the devices in elevated temperatures. Therefore, the corrosive environment must be taken into consideration when designing geophones and computer cases.

To prevent corrosion, the chip of the geophone is firstly wrapped by a plastic shell and a metal inner shell. An anti-corrosive outer shell is then applied to protect the whole structure of the geophone, as shown in **Figs. 14 and 15**.

C. IDENTIFICATION AND LOCATION OF MICROSEISMIC EVENTS

Ten geophones were installed at levels −690 m, −765 m, and −780 m, respectively, as shown in **Fig. 16**. A variety of microseismic signals were received during tunneling, among which a large proportion were interfering signals induced by blasting, electric pulse and the electric fan, as shown in **Fig. 17**. The microseismic signals can be recognized and filtered out by comparing the wave forms and conducting spectral analysis. Then, the source location was calculated using the filtered microseismic signals trough the Geiger iteration algorithm [37]:

$$\sqrt{(x - x_i)^2 + (y - y_i)^2 + (z - z_i)^2} = v_p(t - t_i) \qquad (3)$$

where $(x_i, y_i, z_i,)$ and (x, y, z, t) are the coordinates of the i-th geophone and seismic source, respectively; v_p represents the P-wave velocity. The initial coordinate of the seismic source is randomly assigned and iterated using least square algorithm until the required accuracy is achieved. The P-wave velocity is calculated by calibration blasting in Sanshandao goldmine. From the calibration results, the P-wave velocities ranged from 4500 m/s to 5500 m/s. The average location error of x, y and z coordinates versus wave velocity was compared to select the optimum P-wave velocity for the microseismic monitoring system (see **Fig. 18**). It can be seen that the optimum P-wave velocity is 5000 m/s with the smallest location error of 10.2 m.

D. ROCKBURST RISK ASSESSMENT BASED ON MICROSEISMIC MONITORING

1) ROCKBURST RISK ASSESSMENT BASED ON SPATIAL-TEMPORAL DISTRIBUTION OF MICROSEISMIC EVENTS

The microseismic monitoring system was installed in December, 2014. **Fig. 19** demonstrates the spatial-temporal distribution of the microseismic events during mining from December, 2014 to March, 2015. It can be seen that 36 and 30 events were captured by the microseismic monitoring system in December, 2014 and January, 2015, respectively, among which a large proportion are low-energy events. This indicates that the rock mass at this mining level is stable. In February, 2015, only 14 microseismic events with low energy were recorded (see **Fig. 19c**). This is because secondary reinforcement was conducted in the roadways. In March, 2015 several large-energy microseismic events were recorded near the crosscut (**Fig. 19d**), which induced a rockburst accident on 31, March, 2015. Some anchors, cables and rock mass were damaged seriously in this accident, as shown in **Fig. 20**.

2) ROCKBURST RISK ASSESSMENT BASED ON MICROSEISMIC ACTIVITY RATE AND ENERGY RELEASE RATE

In order to ensure mining safety, it is insufficient to analyze the spatial-temporal distribution of the microseismic events only. The microseismic monitoring system is required

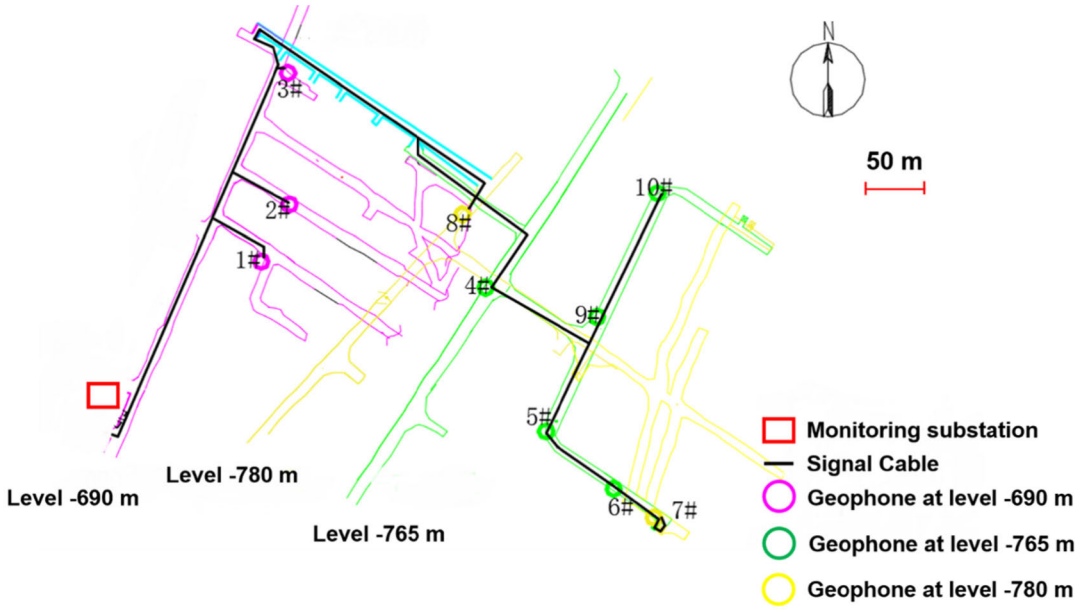

FIGURE 16. Sensor deployment at Levels −690 m, −765 m, and −780 m in Sanshandao goldmine.

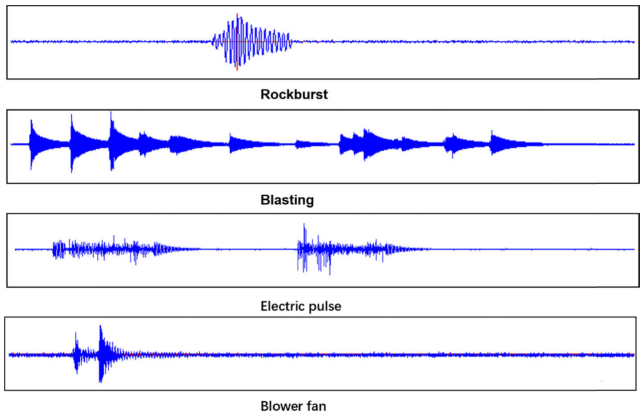

FIGURE 17. Typical wave forms of the microseismic signal and interfering signals.

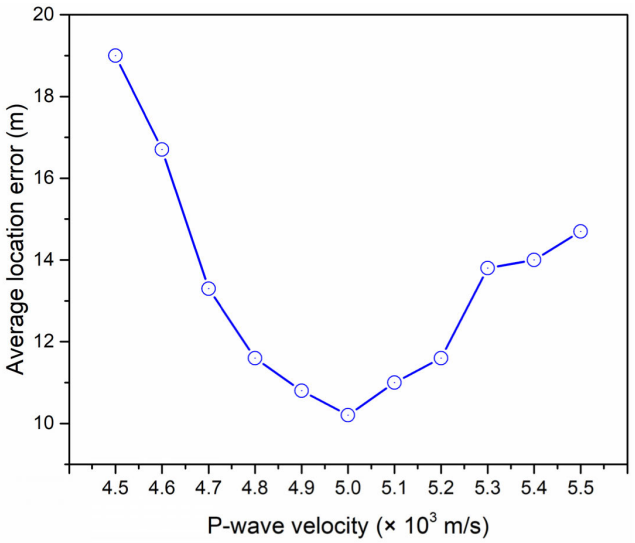

FIGURE 18. Location error versus p-wave velocity.

to be able to analyze the change of event count and energy in real time to predict the possible time of rockburst occurrence.

The microseismic activity rate and energy release rate are the changes of the event number and event energy, respectively [38]. The sudden increase of microseismic event number indicates that the rock mass is fracturing. It can be seen from **Fig. 21 a–d** that the event energy is positively correlated with the event number. Rockburst is very likely to occur when both the event number and event energy increase simultaneously. Also, the energy saltation always lags behind the number saltation of the microseismic events. Usually, sudden changes in energy often indicate the occurrence of rockburst disasters. Therefore, real-time analysis of microseismic activity rates can obtain the trend of the energy release rate, which is convenient for predicting the occurrence time of rockburst. It can be observed from **Fig. 21**e that the whole period from December 2014 to March 2015 can be divided into four subperiods: stationary period, active period, secondary stationary period and secondary active period. In the stationary period, the total number and energy of microseismic events are small because there are no tunneling and mining activity in this period; in the active period, the total number and energy of microseismic events increase suddenly due to tunneling; in the secondary stationary period, the total number and energy of microseismic events fluctuate within a small range due to shotcrete support; and in the secondary active period, the total number and energy of microseismic events increase suddenly again due to mining at level −780 m. The results agree well with the mining activity in the mine.

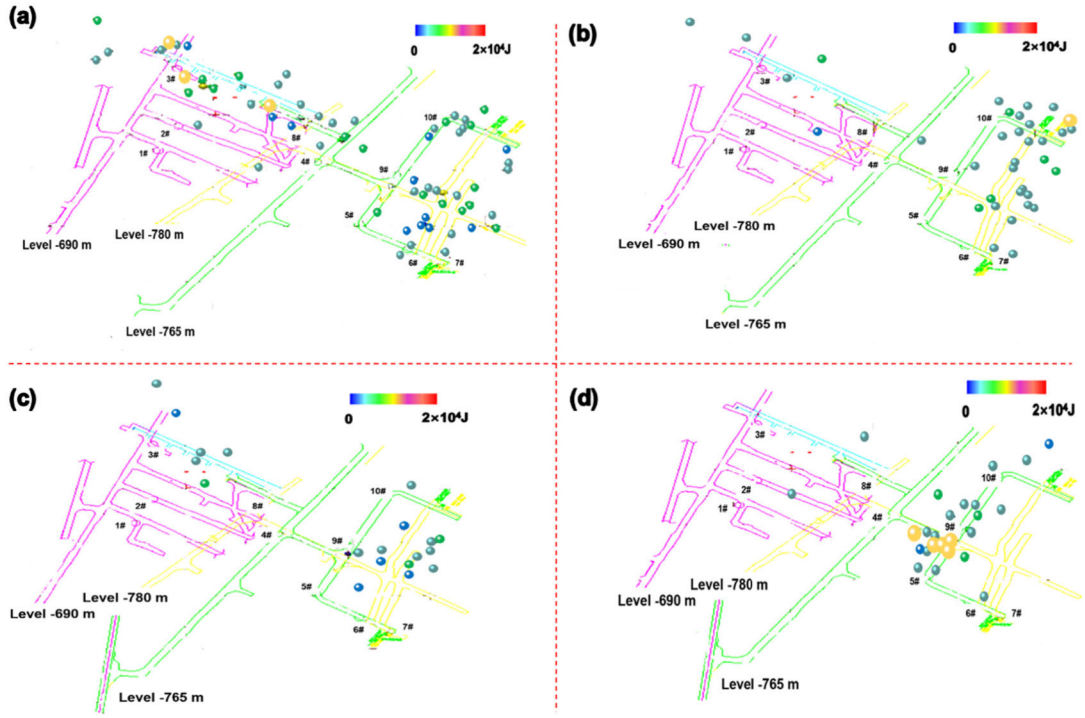

FIGURE 19. Spatial-temporal distribution of microseismic events in (a) December, 2014; (b) January, 2015; (c) February, 2015; (d) March 2015.

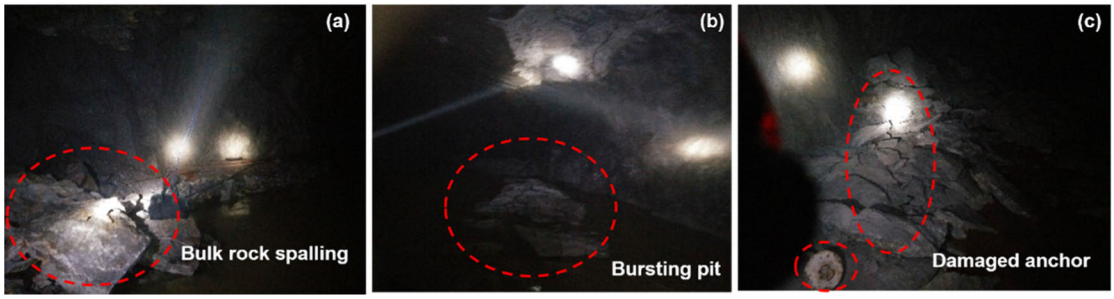

FIGURE 20. Photos of the rockburst accident.

3) ROCKBURST RISK ASSESSMENT BASED ON CONTINUITY INDEX AND AVERAGE DAILY ENERGY

If microseismic events are continuously generated for a period of time, rockburst is likely to occur. In order to characterize the daily continuity of microseismic events, the continuity index is introduced in this study. It is defined as the ratio of the total number of events received since the system was established to the number of days, which can be expressed as:

$$U = \frac{\sum N_D}{D} \tag{4}$$

where N_D is the total number of microseismic events on the Dth day; D is the number of continuous monitoring days. It is known that rockburst is induced mainly by large-energy microseismic events. Large daily energy release may not cause rockburst if there exists a large number of small-energy events. To address this problem, this study introduces average daily energy:

$$\overline{EI}_D = \frac{\sum EI}{N_D} \tag{5}$$

where $\sum EI$ is the total daily energy of microseismic events; N_D is the total daily number of microseismic events.

Fig. 22 shows statistics of continuity index and average daily energy from December, 2014 to March, 2015, which can be also divided into four periods (the same as **Fig. 21**). A sudden change of continuity index and average daily energy can be observed in the active period in comparison with the stationary period. Minor rockbursts constantly occurred, which induced roadway spalling, rock bolt failure and roadway deformation. In the secondary stationary period, the continuity index constantly decreases and the average

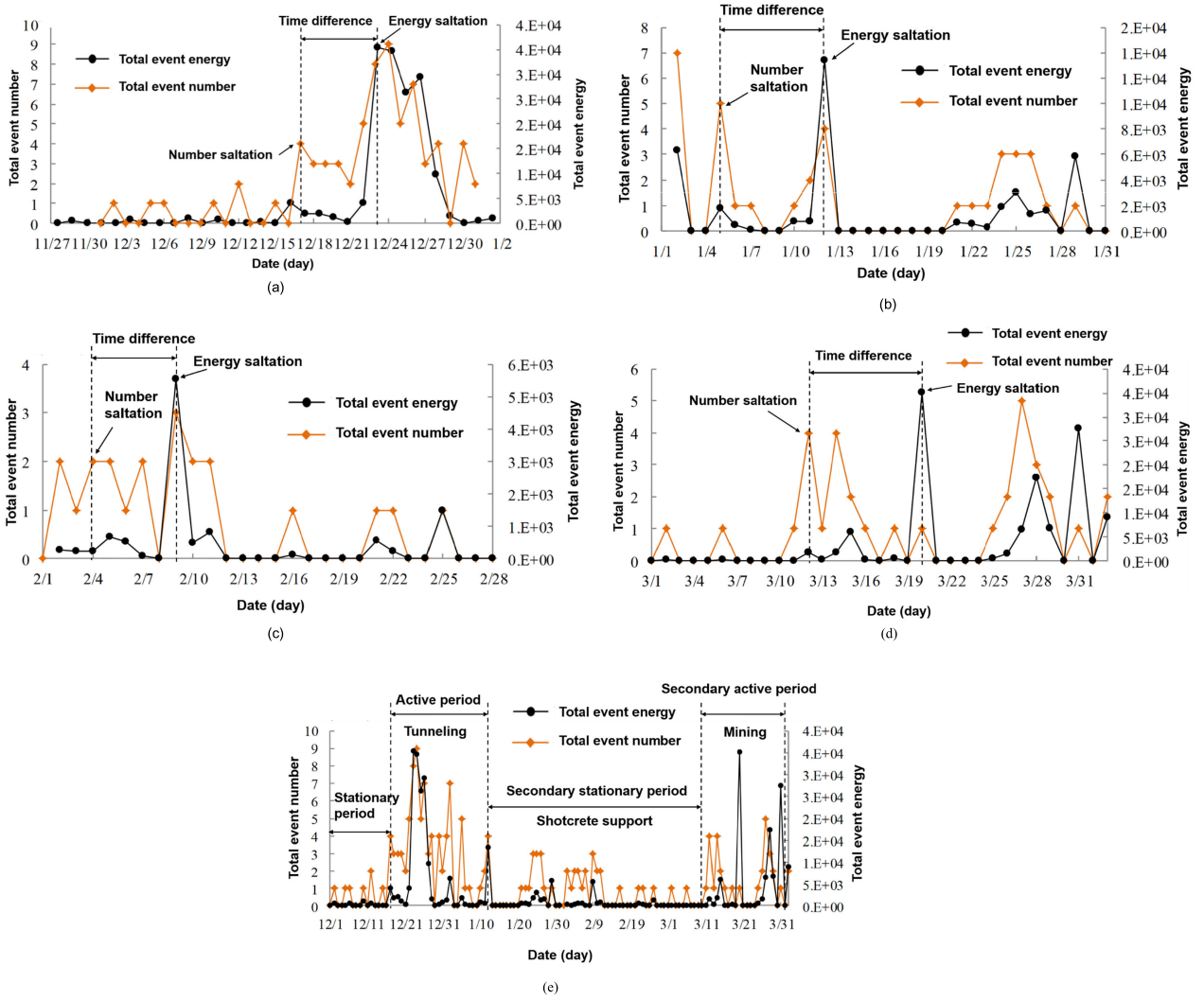

FIGURE 21. Statistics of total event count and energy during December, 2014 (a), January, 2015 (b), February, 2015 (c), March, 2015 (d), and between December, 2014 to March, 2015 (e).

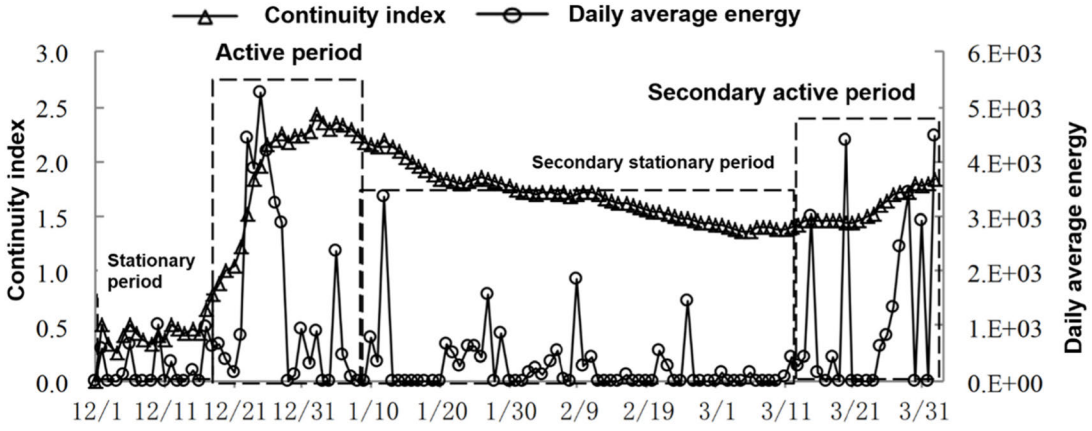

FIGURE 22. Statistics of continuity index and daily average energy from December, 2014 to March, 2015.

daily energy fluctuates within a small range, indicating no risk of rockburst. In the secondary active period (after, 10, March, 2015), the continuity index and average daily energy increase again and, indicating this mine was facing high risk of rockburst. The rockburst that occurred on 31, March, 2015 agrees with the analysis.

V. CONCLUSIONS

Rockburst hazards were monitored using a self-developed microseismic monitoring system in a deep-sea mine. In addition, the propagation patterns of microseismic waves influenced by geological defects have been studied using a similar material simulation model.

The following conclusions are drawn:

- A microseismic monitoring system with anticorrosive equipment is developed for assessing rockburst hazards in undersea mines.
- Geological defects (goafs and faults) will cause amplitude and velocity attenuation of elastic waves, while after back filling, the wave attenuation can be reduced;
- From microseismic monitoring results, the surrounding rock went through four periods: stationary, active, secondary stationary and secondary active periods. Compared with the stationary period, a sudden change of continuity index and average daily energy can be observed in the active period in which minor rockbursts constantly occurred. Rockburst accidents are very likely to occur in the secondary active period. However, before this period, there usually exists a secondary stationary period without rockburst risk.

The microseismic monitoring results obtained in this study agree well with feedback of rockburst accidents that occurred in Sanshandao goldmine. This method is applicable in other deep-sea mines with similar geological conditions. However, various geological factors can affect microseismic wave propagation, such as joints, bedding, subsided columns, rock intrusion and lithological variation. The wave propagation patterns need to be further analyzed when applying the microseismic monitoring system in mines with such geological conditions. In the future work, other seismic parameters, such as energy index, cumulative apparent volume, Schmidt number, etc. will be further investigated to predict rockburst hazards.

ACKNOWLEDGMENT

(Dong Li and Junfei Zhang are co-first authors.)

REFERENCES

[1] P. K. Kaiser, *Canadian Rockburst Support Handbook*, Geomechanics Res. Centre, Laurentian Univ., Sudbury, ON, Canada, 1996.
[2] T. Li, M. F. Cai, and M. Cai, "A review of mining-induced seismicity in China," *Int. J. Rock Mech. Mining Sci.*, vol. 44, no. 8, pp. 1149–1171, Dec. 2007.
[3] J. Zhang, F. Jiang, J. Yang, W. Bai, and L. Zhang, "Rockburst mechanism in soft coal seam within deep coal mines," *Int. J. Mining Sci. Technol.*, vol. 27, no. 3, pp. 551–556, May 2017.
[4] Z. Wen, S. Jing, Y. Jiang, L. Tian, J. Wen, Z. Cao, S. Shi, and Y. Zuo, "Study of the fracture law of overlying strata under water based on the flow-stress-damage model," *Geofluids*, vol. 2019, May 2019, Art. no. 3161852.
[5] A. Keneti and B.-A. Sainsbury, "Review of published rockburst events and their contributing factors," *Eng. Geol.*, vol. 246, pp. 361–373, Oct. 2018.
[6] S. Li, X.-T. Feng, Z. Li, B. Chen, C. Zhang, and H. Zhou, "*In situ* monitoring of rockburst nucleation and evolution in the deeply buried tunnels of Jinping II hydropower station," *Eng. Geol.*, vols. 137–138, pp. 85–96, Jun. 2012.
[7] K. Ma, C. A. Tang, Z. Z. Liang, D. Y. Zhuang, and Q. B. Zhang, "Stability analysis and reinforcement evaluation of high-steep rock slope by microseismic monitoring," *Eng. Geol.*, vol. 218, pp. 22–38, Feb. 2017.
[8] M. Salvoni and P. Dight, "Rock damage assessment in a large unstable slope from microseismic monitoring—MMG Century mine (Queensland, Australia) case study," *Eng. Geol.*, vol. 210, pp. 45–56, Aug. 2016.
[9] Z. Wen, E. Xing, S. Shi, and Y. Jiang, "Overlying strata structural modeling and support applicability analysis for large mining-height stopes," *J. Loss Prevention Process Industries*, vol. 57, pp. 94–100, Jan. 2019.
[10] Y. Fan, W. Lu, Y. Zhou, P. Yan, Z. Leng, and M. Chen, "Influence of tunneling methods on the strainburst characteristics during the excavation of deep rock masses," *Eng. Geol.*, vol. 201, pp. 85–95, Feb. 2016.
[11] F. Song, H. S. Kuleli, M. N. Toksöz, E. Ay, and H. Zhang, "An improved method for hydrofracture-induced microseismic event detection and phase picking," *Geophysics*, vol. 75, no. 6, pp. A47–A52, Oct. 2010.
[12] F. Song and M. N. Toksöz, "Full-waveform based complete moment tensor inversion and source parameter estimation from downhole microseismic data for hydrofracture monitoring," *Geophysics*, vol. 76, no. 6, pp. WC103–WC116, Nov. 2011.
[13] Q. Zhu, Y. Feng, M. Cai, J. Liu, and H. Wang, "Interpretation of the extent of hydraulic fracturing for rockburst prevention using microseismic monitoring data," *J. Natural Gas Sci. Eng.*, vol. 38, pp. 107–119, Feb. 2017.
[14] C. A. Tang, J. Wang, and J. Zhang, "Preliminary engineering application of microseismic monitoring technique to rockburst prediction in tunneling of Jinping II project," *J. Rock Mech. Geotech. Eng.*, vol. 2, no. 3, pp. 193–208, Sep. 2010. doi: 10.3724/SP.J.1235.2010.00193.
[15] V. Falmagne, P. K. Kaiser, and C. D. Martin, "Microseismic monitoring and rock mass degradation," in *Proc. 100th Can. Inst. Mining Metall. Annu. Gen. Meeting (CD-ROM)*, Montreal, QC, Canada, 1998, pp. 1–8.
[16] J. Zhang, F. Jiang, S. Zhu, and L. Zhang, "Width design for gobs and isolated coal pillars based on overall burst-instability prevention in coal mines," *J. Rock Mech. Geotech. Eng.*, vol. 8, no. 4, pp. 551–558, Aug. 2016.
[17] N. G. W. Cook, "Seismicity associated with mining," *Eng. Geol.*, vol. 10, nos. 2–4, pp. 99–122, Dec. 1976.
[18] X. Wang, Z. Wen, Y. Jiang, and H. Huang, "Experimental study on mechanical and acoustic emission characteristics of rock-like material under non-uniformly distributed loads," *Rock Mech. Rock Eng.*, vol. 51, no. 3, pp. 729–745, Mar. 2018.
[19] A. Reshetnikov, S. Buske, and S. Shapiro, "Seismic imaging using microseismic events: Results from the San Andreas fault system at SAFOD," *J. Geophys. Res.*, p. 115, 2010.
[20] I. Das and M. D. Zoback, "Long-period, long-duration seismic events during hydraulic fracture stimulation of a shale gas reservoir," *Lead. Edge*, vol. 30, no. 7, pp. 778–786, 2011.
[21] M. Ujihira, T. Isobe, and K. Higuchi, "On the flaking destructive phenomena of porous material induced by involved high pressure gas," *J. Mining Metall. Inst. Jpn.*, vol. 100, no. 1153, pp. 225–232, 1984. doi: 10.2473/shigentosozai1953.100.1153_225.
[22] M. Ujihira, T. Isobe, and K. Higuchi, "On the proeess of destruction of porous material in which high pressure gas is involved," *J. Mining Metall. Inst. Jpn.*, vol. 100, no. 5, pp. 397–403, 1984. doi: 10.2473/shigentosozai1953.100.1155_397.
[23] Q. Hu, S. Zhang, G. Wen, L. Dai, and B. Wang, "Coal-like material for coal and gas outburst simulation tests," *Int. J. Rock Mech. Mining Sci.*, vol. 74, pp. 151–156, Feb. 2015. doi:10.1016/j.ijrmms.2015.01.005.
[24] M.-G. Zhai and M. Santosh, "The early precambrian odyssey of the north china craton: A synoptic overview," *Gondwana Res.*, vol. 20, no. 1, pp. 6–25, Jul. 2011.
[25] L. Wang, Y. M. Qiu, N. J. McNaughton, D. I. Groves, Z. K. Luo, J. Z. Huang, L. C. Miao, and Y. K. Liu, "Constraints on crustal evolution and gold metallogeny in the Northwestern Jiaodong Peninsula, China, from SHRIMP U–Pb zircon studies of granitoids," *Ore Geol. Rev.*, vol. 13, nos. 1–5, pp. 275–291, Apr. 1998.
[26] X.-C. Li, H.-R. Fan, M. Santosh, F.-F. Hu, K.-F. Yang, and T.-G. Lan, "Hydrothermal alteration associated with mesozoic granite-hosted gold mineralization at the sanshandao deposit, jiaodong gold province, China," *Ore Geol. Rev.*, vol. 53, pp. 403–421, Sep. 2013. doi: 10.1016/j.oregeorev.2013.01.020.
[27] W.-G. Xu, H.-R. Fan, K.-F. Yang, F.-F. Hu, Y.-C. Cai, and B.-J. Wen, "Exhaustive gold mineralizing processes of the Sanshandao gold deposit, Jiaodong Peninsula, eastern China: Displayed by hydrothermal alteration modeling," *J. Asian Earth Sci.*, vol. 129, pp. 152–169, Nov. 2016.
[28] M. Cai, "Prediction and prevention of rockburst in metal mines—A case study of Sanshandao gold mine," *J. Rock Mech. Geotech. Eng.*, vol. 8, no. 2, pp. 204–211, Apr. 2016.

[29] H. Kang, "Support technologies for deep and complex roadways in underground coal mines: A review," *Int. J. Coal Sci. Technol.*, vol. 1, no. 3, pp. 261–277, Sep. 2014.
[30] D. Huayang, L. Xugang, L. Jiyan, L. Yixin, Z. Yameng, D. Weinan, and C. Yinfei, "Model study of deformation induced by fully mechanized caving below a thick loess layer," *Int. J. Rock Mech. Mining Sci.*, vol. 6, no. 47, pp. 1027–1033, 2010.
[31] W. Ren, C. Guo, Z. Peng, and Y. Wang, "Model experimental research on deformation and subsidence characteristics of ground and wall rock due to mining under thick overlying terrane," *Int. J. Rock Mech. Mining Sci.*, vol. 47, no. 4, pp. 614–624, Jun. 2010.
[32] H. Kong, L. Wang, G. Gu, and B. Xu, "Application of DICM on similar material simulation experiment for rock-like materials," *Adv. Civil Eng.*, vol. 2018, Apr. 2018, Art. no. 5634109.
[33] Q. Ye, G. Wang, Z. Jia, C. Zheng, and W. Wang, "Similarity simulation of mining-crack-evolution characteristics of overburden strata in deep coal mining with large dip," *J. Petroleum Sci. Eng.*, vol. 165, pp. 477–487, Jun. 2018.
[34] K. Wu, G.-L. Cheng, and D.-W. Zhou, "Experimental research on dynamic movement in strata overlying coal mines using similar material modeling," *Arabian J. Geosci.*, vol. 8, no. 9, pp. 6521–6534, Sep. 2015.
[35] K. T. Law, Y. Cao, and G. He, "An energy approach for assessing seismic liquefaction potential," *Can. Geotech. J.*, vol. 27, no. 3, pp. 320–329, Jun. 1990.
[36] S. Chapman, B. Quintal, N. Tisato, and K. Holliger, "Frequency scaling of seismic attenuation in rocks saturated with two fluid phases," *Geophys. J. Int.*, vol. 208, no. 1, pp. 221–225, Jan. 2017.
[37] A. F. Prugger and D. J. Gendzwill, "Microearthquake location: A nonlinear approach that makes use of a simplex stepping procedure," *Bull. Seismological Soc. Amer.*, vol. 78, no. 2, pp. 799–815, Apr. 1988.
[38] C.-L. Wang, "Identification of early-warning key point for rockmass instability using acoustic emission/microseismic activity monitoring," *Int. J. Rock Mech. Mining Sci.*, vol. 100, no. 71, pp. 171–175, 2014.

DONG LI received the B.S. and M.S. degrees from the Shandong University of Technology, Shandong, China, and the Ph.D. degree in mining engineering from the University of Science and Technology Beijing, Beijing, China, in 2019, all in mining engineering. He is currently a Lecturer with the North China Institute of Science and Technology. His research interests include the evaluation of dynamic hazards in deep mines using seismic monitoring techniques and the advanced numerical simulation methods.

JUNFEI ZHANG received the B.S. and M.S. degrees in mining engineering from the University of Science and Technology Beijing, Beijing, China. He is currently pursuing the Ph.D. degree with the Department of Civil, Environmental, and Mining Engineering, University of Western Australia. His main research interests include the evaluation of geotechnical hazards using monitoring techniques and machine learning algorithms.

CUNWEN WANG received the B.S. and M.S. degrees from the Shandong University of Technology, Shandong, China, and the Ph.D. degree from the University of Science and Technology Beijing, Beijing, China, in 2009, all in mining engineering. He is currently a Senior Researcher with the Rock Burst Research Centre, Shandong Energy Group Company Ltd. His research interests include the area of rock burst mechanism, mitigation, monitoring, and early-warning.

YANG CHEN received the B.S. degree in architectural environment and equipment engineering and the M.S. degree in mining engineering from the Shandong University of Technology, Shandong, China. He is currently pursuing the Ph.D. degree with the School of Civil and Resources Engineering, University of Science and Technology Beijing, Beijing, China. His research interests include the mechanism and prevention of coal burst under the condition of complicated overburden strata using microseismic monitoring techniques and physical simulation methods.

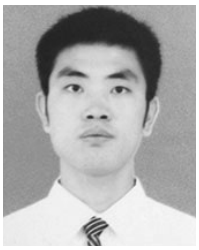

DECHENG GE received the B.S. and M.S. degrees in mining engineering from the Shandong University of Technology, Shandong, China. He is currently pursuing the Ph.D. degree in mining engineering with the University of Science and Technology Beijing, Beijing, China. His main research interests include the evaluation of dynamic hazards in deep mines using seismic monitoring techniques and the advanced numerical simulation methods.